Title

Role of WW Domain-containing Oxidoreductase WWOX in Driving T Cell Acute Lymphoblastic Leukemia Maturation*

Authors

Huang, Shenq-Shyang
Su, Wan-Pei
Lin, Hsin-Pin
et al.

Role of WW Domain-containing Oxidoreductase WWOX in Driving T Cell Acute Lymphoblastic Leukemia Maturation*[S]

Shenq-Shyang Huang[‡], Wan-Pei Su[‡], Hsin-Pin Lin[‡], Hsiang-Ling Kuo[‡], Hsiao-Ling Wei[‡], and Nan-Shan Chang[‡§¶‖**‡‡1]

From the [‡]Institute of Molecular Medicine, [§]Center of Infectious Disease and Signaling Research, and [¶]Advanced Optoelectronic Technology Center, National Cheng Kung University, Tainan 70101, Taiwan, Republic of China, [‖]Department of Neurochemistry, New York State Institute for Basic Research in Developmental Disabilities, Staten Island, New York, New York 10314, [**]Department of Neuroscience and Physiology, SUNY Upstate Medical University, Syracuse, New York 13210, [‡‡]Graduate Institute of Biomedical Sciences, College of Medicine, China Medical University, Taichung 40402, Taiwan, Republic of China

Whether tumor suppressor WWOX (WW domain-containing oxidoreductase) stimulates immune cell maturation is largely unknown. Here, we determined that Tyr-33-phosphorylated WWOX physically binds non-phosphorylated ERK and IκBα in immature acute lymphoblastic leukemia MOLT-4 T cells and in the naïve mouse spleen. The IκBα·ERK·WWOX complex was shown to localize, in part, in the mitochondria. WWOX prevents IκBα from proteasomal degradation. Upon stimulating MOLT-4 with ionophore A23187/phorbol myristate acetate, endogenous IκBα and ERK undergo rapid phosphorylation in <5 min, and subsequently WWOX is Tyr-33 and Tyr-287 de-phosphorylated and Ser-14 phosphorylated. Three hours later, IκBα starts to degrade, and ERK returns to basal or non-phosphorylation, and this lasts for the next 12 h. Finally, expression of CD3 and CD8 occurs in MOLT-4 along with reappearance of the IκBα·ERK·WWOX complex near 24 h. Inhibition of ERK phosphorylation by U0126 or IκBα degradation by MG132 prevents MOLT-4 maturation. By time-lapse FRET microscopy, IκBα·ERK·WWOX complex exhibits an increased binding strength by 1–2-fold after exposure to ionophore A23187/phorbol myristate acetate for 15–24 h. Meanwhile, a portion of ERK and WWOX relocates to the nucleus, suggesting their role in the induction of CD3 and CD8 expression in MOLT-4.

The pathway by which T cells differentiate via various stages of selection has been well documented (1). Briefly, bone marrow pluripotent hematopoietic stem cell differentiates into precursor T cell and then migrates to the thymus. In mouse thymus, precursor T cell (CD44^{low}) differentiates into CD4-CD8 double-negative cell and then goes through four stages, namely stage I CD44+CD25-, stage II CD44+ CD25+, stage III CD44-CD25+ with pre-TCR[2] (pre-T cell receptor) expression, and stage IV CD44-CD25− (1). After stage IV, double-negative cells differentiate into CD4/CD8 double-positive cells with TCR (T cell receptor) expression. The CD4 and CD8 single-positive cells, regulatory T cells (Treg), and natural killer-like T cells (NKT) are generated after further positive and negative selection (2, 3). In comparison, human hematopoietic progenitor cells, possessing CD34, CD7, and CD5 markers, undergo similar developmental stages to become mature T cells (4, 5).

T cell receptor-β and -α (TCR-β/α) subunits form a complex on the cell membrane in the double-negative stage. The surface CD3 complex expression level is elevated during double-positive to single-positive transition (1). TCR-β/α and CD3 complexes on the cell surface receive stimulatory signals from major histocompatibility complex (MHC) for triggering the downstream activation cascade for cell maturation and activation (6). MAPK pathway is implicated in the positive/negative selection involving TCRα, CD3γ, CD3δ, and PLCγ1. Positive selection results from a low, sustained level of ERK activation, whereas negative selection occurs in response to a large burst of ERK activation concomitant with JNK and p38 activation (1).

Substantial evidence shows that nuclear factor κB (NF-κB) and its inhibitors (IκB) are involved in the T cell maturation (7). IκBα induces a limited number of double-positive CD4^{+} CD8^{+} cells (8). Transgenic mice expressing a superinhibitory form of IκBα (IκB$\alpha_{\Delta32/36}$) have an increased number of CD4^{+} CD8^{+} double-positive cells but decreased number of CD4^{+} or CD8^{+} single-positive cells (9). A low level of calcium ionophore A23187 and 12-myristate 13-acetate (PMA), designated IoP hereafter, is known to induce the differentiation of mononuclear cells, human T-lymphoblastic cell lines HPB-ALL and MOLT-3, and normal lymphocytes (10). Indeed, IoP replaces TCR signals to induce positive selection of CD4^{+} T cells (11). In contrast, PMA induces apoptosis of T cells at micromolar concentrations (12).

The upstream signal preceding the aforementioned MAPK/NF-κB pathway is largely unknown during T cell differentia-

[2] The abbreviations used are: TCR, T cell receptor; dn, dominant negative; NF-κB, nuclear factor κB; PMA, 12-myristate 13-acetate; DsRed, *Discosoma* sp. red fluorescent protein; ECFP, enhanced cyan fluorescent protein; EGFP, enhanced green fluorescent protein; EYFP, enhanced yellow fluorescent protein; IκBα, inhibitor of NF-κB; IoP, ionophore A23187/phorbol myristate acetate; WWOX, WW domain-containing oxidoreductase.

tion. Here, we investigated whether tumor suppressor WW domain-containing oxidoreductase, known as WWOX, FOR, or WOX1, participates in the early signaling of T cell acute lymphoblastic leukemia (T-ALL) maturation. WWOX plays a crucial role in tumor suppression, metabolism, ataxia, epilepsy, neural disorders, neuronal damages and degeneration, and anti-viral immune responses (13–22). Here, we showed that WWOX binds IκBα and ERK and the complex localizes, in part, in the mitochondria of immature T lymphoid cells. IoP rapidly induces IκBα and ERK phosphorylation to cause dissociation of the IκBα·ERK·WWOX complex that ultimately leads to nuclear localization of WWOX and ERK.

Experimental Procedures

Cell Lines—Human T cell acute lymphoblastic leukemia MOLT-4 and Jurkat cells, monocytic U937 and THP-1 cells, breast MDA-MB-231 cancer cells, and embryonic HEK293 fibroblasts were from American Type Culture Collections (ATCC, Manassas, VA) and cultured according to the provider's instructions.

Chemicals and Antibodies—PMA, 1,4-diamino-2,3-dicyano-1,4-bis(2-aminophenylthio)butadiene (U0126), and ionophore A23187 were from Sigma. Commercial antibodies used were: polyclonal ERK1, ERK2, WWOX (Santa Cruz Biotechnology), and lamin A/C (Cell Signaling); monoclonal p-ERK, NF-κB/p65, and CD3 (Santa Cruz Biotechnology), IκBα (Epitomics), and cell cycle antibody kit (BD Pharmingen). We made specific antibodies against WWOX and phosphorylation sites Tyr(P)-287, Ser(P)-14, and Tyr(P)-33 as described (21–26). A synthetic peptide for Tyr(P)-61 antibody production was NH-CVAGD-LP**pY**GWEGETDEN-COOH. A control non-phosphorylated peptide was NH-CVAGDLPYGWEGETDEN-COOH.

DNA Constructs—Murine full-length WWOX and dominant-negative (dn) cDNA constructs were made as described (21, 22). Expression constructs for murine IκBα (1–301), IκBα295N-(1–295), and IκBα243C-(244–295) were made in pECFP-C1 vector (cloning site, EcoRI) (27). Additional IκBα clones were made in pECFP-C1 using the following primer sets: 1) IκBα-(1–243): forward, CCGAATTCCATGTTTCAGCC; reverse, TAGAATTCGACATCAGCCCC; 2) IκBα-(1–67): forward, CCGAATTCTATGTTTCAGCCAG; reverse, TAGAATT CCTTCCAGGGCTC; 3) IκBα-(68–243): forward, CC-GAATTCTCAGCAGCTCAC; reverse, ATGAATTCGACAT-CAGCCCC; 4) IκBα-(244–314): forward, CCAAGCTTTTA-ACAGGGTAACC; reverse, GGAAGCTTTTATAATGTCA-GACGC. The established constructs were introduced in MOLT-4 and Jurkat cells by electroporation using 2.5 to 15 μg of DNA constructs (220 V and 50 ms using the BTX ECM 630 electroporator, Genetronics, San Diego, CA).

Förster (Fluorescence) Resonance Energy Transfer (FRET)—FRET microscopy was carried out as previously described (25, 26, 28, 29). MOLT-4 cells were transiently overexpressed with ECFP-IκBα (or other indicated constructs) and EYFP-WWOX expression constructs and cultured for 24–36 h. FRET analysis was performed using an inverted fluorescence microscope (Nikon Eclipse TE-2000U). Cells were stimulated with an excitation wavelength 440 nm. FRET signals were detected at an emission wavelength 535 nm. ECFP and EYFP were used as

donor and acceptor fluorescent molecules, respectively. The FRET images were corrected for background fluorescence from an area without cells and spectral bleed-through. The spectrally corrected FRET concentration (FRETc) was calculated by Youvan's equation (using a software program Image Pro 6.1, Media Cybernetics): FRETc = (fret − bk[fret] − cf[don] × (don − bk[don] − cf[acc] × (acc-bk[acc]), where fret = fret image, bk = background, cf = correction factor, don = donor image, and acc = acceptor image. The equation normalizes the FRET signals to the expression levels of the proteins. Where indicated, time-lapse microscopy for FRET was carried out to determine IoP-regulated binding interactions among ECFP-IκBα, EGFP-ERK, and DsRed-WWOX, as described (29). An inverted Olympus IX81 fluorescence microscope and the internal software for FRET analysis were used. As a negative control, a dominant-negative EGFP-ERK(K71R/K72R) (or dn-EGFP-ERK) was generated and used to replace the wild type EGFP-ERK.

Co-immunoprecipitation, Western Blotting, and Immunofluorescence Microscopy—MOLT-4 and Jurkat T cell were exposed to IoP for indicated times, lysed with a lysis buffer (0.5% Nonidet P-40, 10% glycerol in PBS), and then cleared with protein-G-Sepharose beads. Aliquots of an indicated IgG antibody were added to the lysates for immunoprecipitation, as described (23, 24, 26). Additionally, cytoplasmic and nuclear extractions were prepared for immunoprecipitation and immunostaining (23, 24, 26). Similarly, cells were treated with IoP for the indicated times followed by immunostaining processing with specific antibodies. Primary antibodies were against ERK1, ERK2, IκBα, and WWOX (Santa Cruz Biotechnology). Fluorescent secondary antibodies, including donkey anti-rabbit Alexa Fluor 488 IgG and donkey anti-goat or -mouse Alexa Fluor 594 IgG (eBioscience) were used for visualization by fluorescent microscopy and confocal microscopy (24–29). Where indicated, mitochondria were stained with MitoTracker Red (Thermo Fisher Scientific) (22, 26).

Naïve BALB/c Mice—Whole spleens were isolated from naïve BALB/c mice and lysed and prepared for co-immunoprecipitation as described above. Use of the animals has been approved by the Intramural Animal Use and Care Committee (IACUC) of the National Cheng Kung University.

Results

Calcium Ionophore/PMA (IoP) Rapidly Induced IκBα and ERK Phosphorylation, Which Led to CD3 Expression in MOLT-4 T Cell—To investigate the role of WWOX in T cell growth and differentiation, MOLT-4 cell was mainly used in this study, with Jurkat T cell for comparison. MOLT-4 is considered less differentiated than Jurkat. We have shown that Jurkat expresses CD3, but MOLT-4 does not (12). A combination of PMA (0.55 nM) and A23187 (0.30 μM) (or IoP) is known to induce differentiation in MOLT-3, mononuclear cells, and HPB-ALL cells (10). When MOLT-4 and Jurkat cells were exposed to IoP for 15 h, expression of CD3 was significantly increased in whole cell lysates in MOLT-4, but not in Jurkat, 15–24 h post stimulation (Fig. 1, *A* and *B*). CD3 is a differentiation marker of T cell whose subunits accumulate in the intracellular compartments of immature thymocytes (2, 30). How-
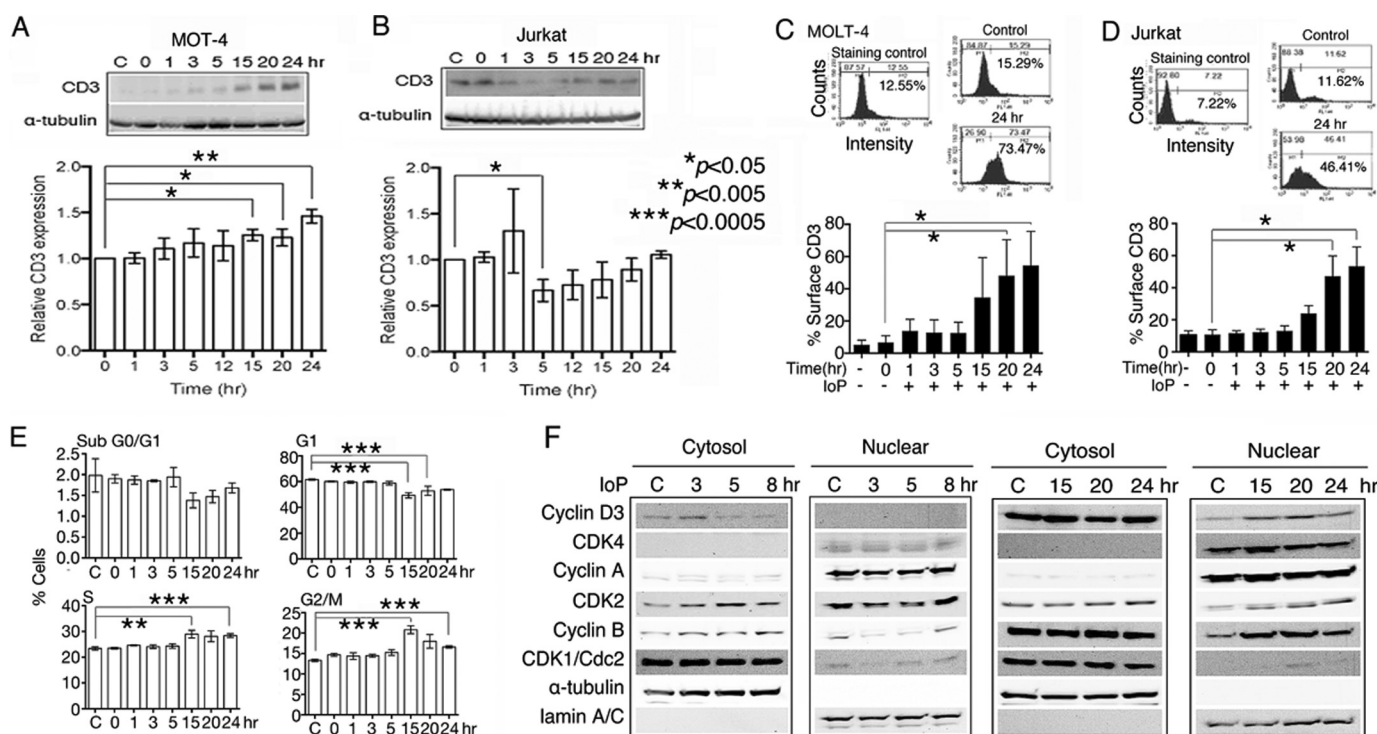
FIGURE 1. **IoP induced ERK phosphorylation and CD3 expression.** *A*, and *B*, MOLT-4 and Jurkat cells were treated with ionophore (0.30 μM)/PMA (0.55 nM) (IoP) for the indicated times. Western blotting analysis was carried out. Student's *t* test is shown for CD3 (mean $\pm$ S.D., $n = 3$; see IκBα data in Fig. 3, *A* and *B*). α-Tubulin was used as an internal loading control. *C* and *D*, MOLT-4 and Jurkat cells were treated with IoP for the indicated times, and non-permeabilized cells were stained at 4 °C with primary mouse anti-CD3 antibody and then FITC-conjugated secondary anti-mouse IgG antibody. In controls, cells were stained with FITC-conjugated anti-mouse IgG antibody alone. Samples were analyzed by flow cytometry (mean $\pm$ S.D., $n = 3$). *E*, IoP-stimulated MOLT-4 cells were shown to enter the S and G$_2$/M phases of the cell cycle. Post IoP stimulation for 15 h increased the percentages of cells entering S and G$_2$/M phase (mean $\pm$ S.D., $n = 3$; Student's *t* test. *F*, expression of cyclins and cyclin-dependent kinases (*CDK*) in MOLT-4 was stained using an antibody kit. G$_2$/M-specific cyclin B in was shown to localize in the nucleus of MOLT-4 post IoP treatment for 15–24 h.

ever, CD3 is on the cell surface of mature cells. IoP significantly increased membrane localization of CD3 in both non-permeabilized MOLT-4 and Jurkat cells after stimulation for 15–24 h as determined by flow cytometry (Fig. 1, *C* and *D*), suggesting that cells have reached maturation. 15 h post stimulation, IoP promoted MOLT-4 to enter the S and G$_2$/M phases of the cell cycle, as determined by flow cytometry (Fig. 1*E*). Also, this is supported by up-regulation and nuclear accumulation of G$_2$/M-specific cyclin B in the IoP-treated MOLT-4 (Fig. 1*F*). The IoP-stimulated cells continued to grow 72 h after exposure (data not shown), which is in agreement with other reports (10, 31).

PMA increased ERK phosphorylation rapidly in 1–3 h and induced differentiation of human myeloblastic leukemia ML-1 cells and Jurkat and MOLT-4 T cells (12, 32). The upstream MEK phosphorylates ERK (p-ERK), whereas p-ERK down-regulates several anti-proliferative genes and promotes the G$_0$/G$_1$ phase to the S phase transition (33, 34). IoP increased ERK phosphorylation at Thr-202 and Tyr-204 in MOLT-4 in 5 min or less, and the phosphorylation lasted for 5 h and was then reduced to a basal level of phosphorylation or non-phosphorylated in 15–24 h (Fig. 2, *A* and *B*). To block MEK/ERK signaling, MOLT-4 cells were pretreated with U0126, a MEK inhibitor, and then exposed to IoP for 24 h. Again, IoP induced CD3 and CD8 expression and ERK phosphorylation (Fig. 2, *C* and *D*). U0126 significantly suppressed ERK and WWOX phosphorylation and abolished CD3 and CD8 expression (Fig. 2, *C* and *D*).

In comparison, human monocytic U937 and THP-1 cells were exposed to IoP. ERK was rapidly phosphorylated in <5 min in both cells (Fig. 2, *E* and *F*). IoP induced CD8α expression in the less differentiated U937 cells in 5 min, whereas the more differentiated THP-1 cells showed a constitutive expression of CD8α (35). In addition, IoP induced the second phase of ERK phosphorylation in both U937 and THP-1, but not in MOLT-4, post stimulation for 15 h (Fig. 2*G*).

IoP Up-regulated Ser-14 Phosphorylation in WWOX and Then Induced IκBα Degradation—In time-course experiments, IoP induced degradation of endogenous IκBα in MOLT-4, which started to occur approximately in 3 h post stimulation (Fig. 3*A*). IκBα disappearance lasted approximately for 12 h. However, IκBα degradation did not occur effectively in the differentiated Jurkat (Fig. 3*B*). When MOLT-4 cells were pretreated with MG-132 for 30 min followed by treating with IoP for 5 h, IκBα degradation was blocked (Fig. 3*C*). Similar experiments were conducted using Jurkat cells, and no degradation of IκBα was observed (Fig. 3*D*).

IoP also affected WWOX phosphorylation. When MOLT-4 cells were exposed to IoP for 10–120 min, there were significant reductions in WWOX phosphorylation at Tyr-33 and Tyr-287, whereas Ser-14 phosphorylation was significantly increased (Fig. 3, *E* and *F*). On the other hand, phosphorylation at Tyr-61 was barely detectable (Fig. 3, *E* and *F*). Phosphorylation at Tyr-33 is needed for WWOX activation and nuclear translocation (21–26), and Tyr-287 phosphorylation is
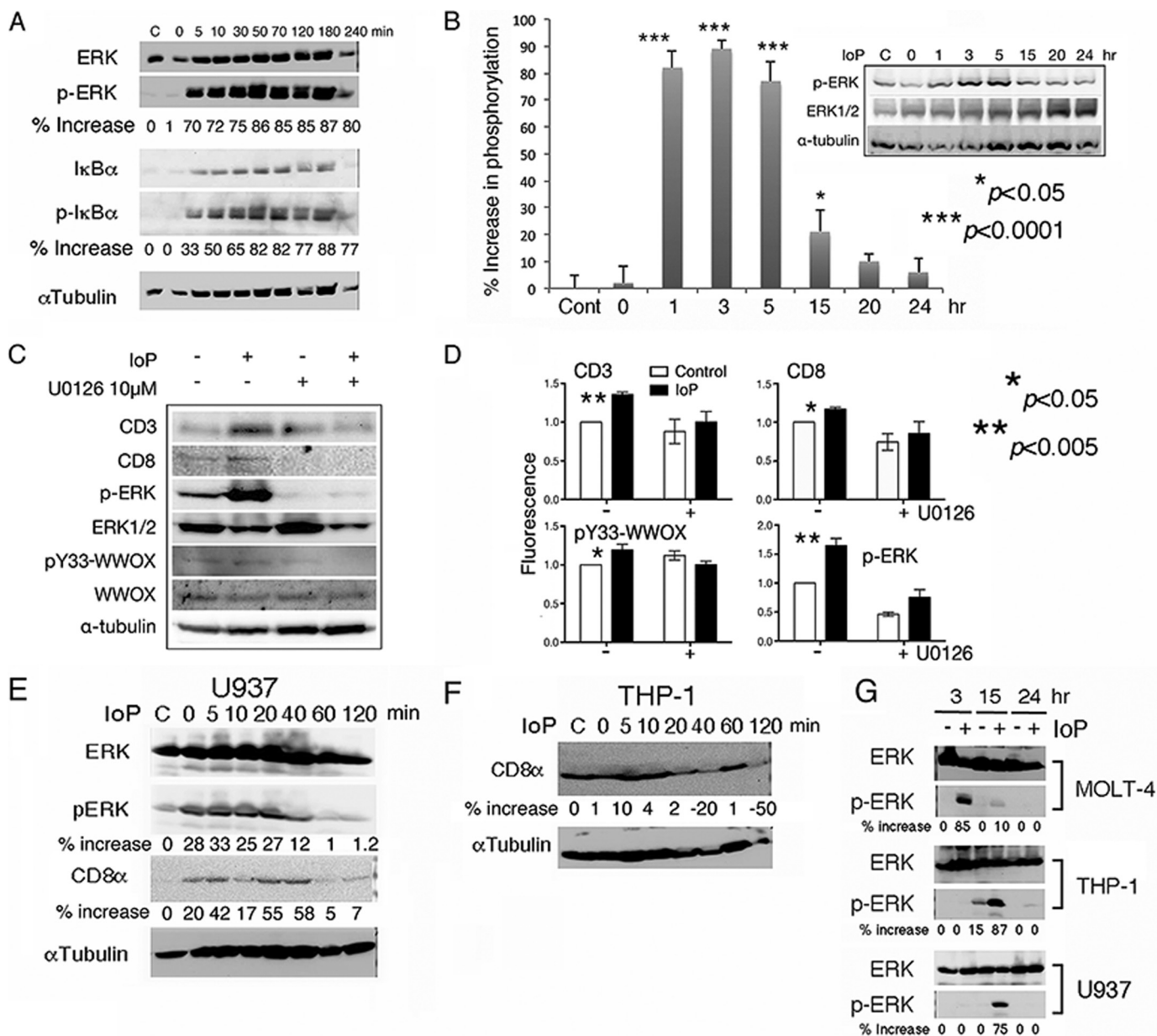
FIGURE 2. **U0126 blocked ERK phosphorylation and IoP-induced MOLT-4 maturation.** *A* and *B*, In time-course experiments, IoP rapidly induced ERK phosphorylation in 5 min or less (in *A*, average of two experiments), and the phosphorylation lasted 15 h in MOLT-4 cells (in *B*, $n = 3$). The *bar graph* shows the normalized p-ERK levels relative to α-tubulin (mean $\pm$ S.D.; $n = 3$). C = non-treated control. *C* and *D*, MOLT-4 cells were pretreated with U0126 (10 μM) for 30 min and then exposed to IoP for 24 h. U0126 blocked the expression of CD3 and CD8 in MOLT-4 T cells (*C*). As shown in the *bar graph* (*D*), IoP significantly increased the expression of CD3 and CD8 and ERK phosphorylation in 24 h and that U0126 suppressed the increases (mean $\pm$ S.D.; $n = 3$). *E* and *F*, human monocytic U937 and THP-1 cells were exposed to IoP and shown to have a rapidly increased ERK phosphorylation in 5 min or less. CD8α expression was induced in the less differentiated U937 cells in 5 min. THP-1 has a constitutive expression of CD8α. *G*, IoP induced the second phase of ERK phosphorylation in U937 and THP-1, but not in MOLT-4, in 15 h post stimulation.

involved in WWOX degradation (36). That is, IoP did not effectively induce WWOX degradation.

The quality of the aforementioned antibodies has been documented (21–26). We rechecked the quality of these homemade antibodies (supplemental Fig. S1). Also, the quality of our newly generated Tyr(P)-61-WWOX antibody is shown.

Using cytosolic and nuclear fractions for Western blotting, we showed that IoP induced translocation of p-ERK to the nuclei in MOLT-4 in 5–7 h post stimulation (Fig. 3*G*). In contrast, no nuclear accumulation of NF-κB/p65 was shown (Fig. 3*G*). WWOX regained phosphorylation at Tyr-33 in 7 h, as it

relocated to the nucleus, whereas nuclear relocation of p-ERK occurred somewhat earlier, which was 5 h after IoP stimulation (Fig. 3*G*).

WWOX Bound IκBα and ERK in the Mitochondria, and IoP Dissociated the WWOX·IκBα·ERK Complex—WWOX is localized in many organelles in resting cells, including mitochondria (22), cell membrane (26), and lysosome (12, 37). Tyr-33-phosphorylated or activated WWOX is mainly localized in the mitochondria and nuclei (21, 22, 23, 38, 39). Translocation of WWOX from the cell membrane, cytoplasm, or lysosome to the mitochondria and nuclei *in vitro* and *in vivo* has been doc-
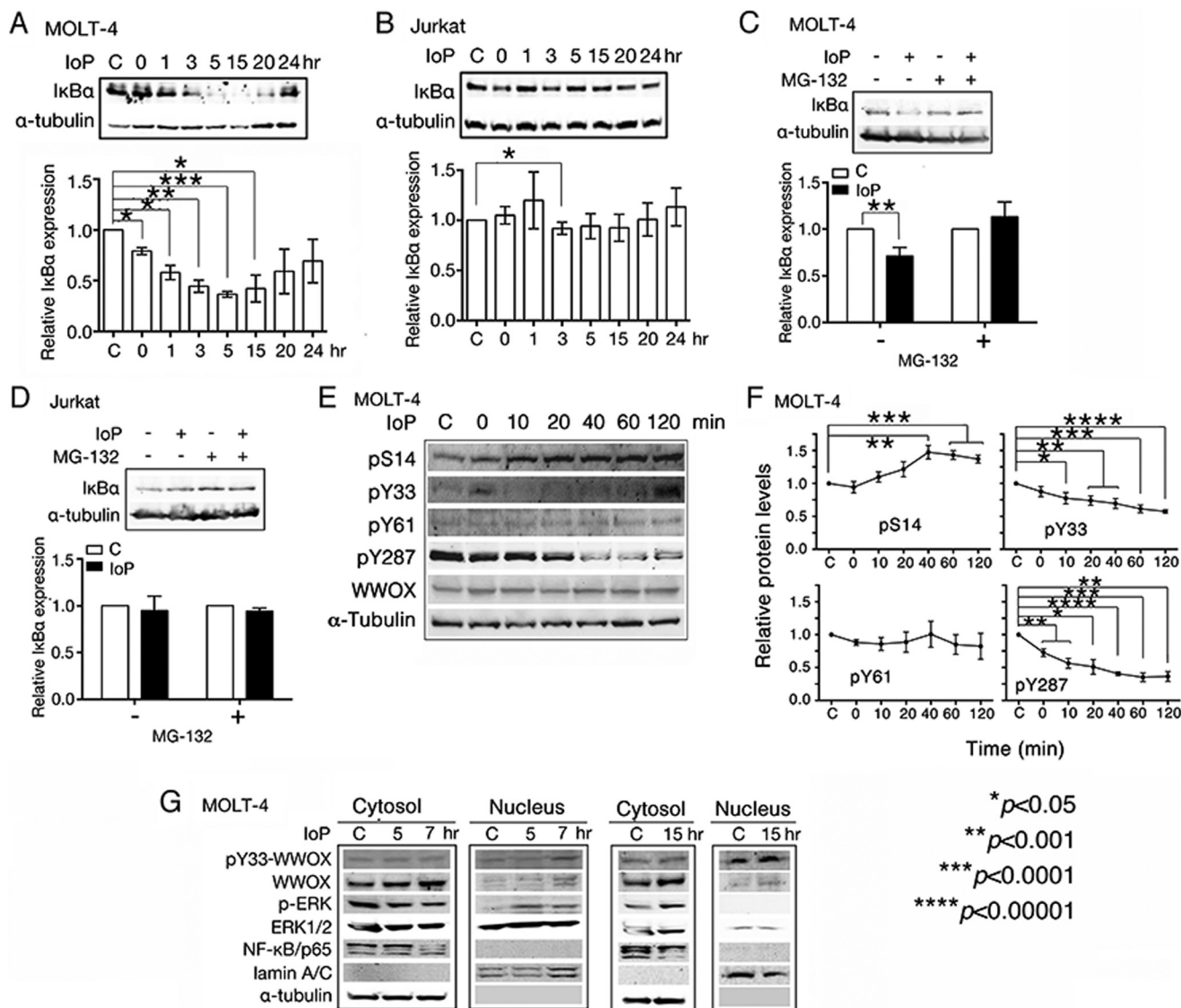
FIGURE 3. IoP rapidly decreased phosphorylation of WWOX at Tyr(P)-33 and Tyr(P)-287 and then induced proteasomal degradation of IκBα in MOLT-4. *A* and *B*, upon stimulating MOLT-4 with IoP, endogenous IκBα became degraded in 3 h, and the degradation lasted in the next 12 h. In contrast, IκBα degradation did not occur effectively in Jurkat. Data are shown as the mean ± S.D.; MOLT-4 *n* = 6, Jurkat *n* = 3. *C* = non-treated control. *C* and *D*, MOLT-4 and Jurkat cells were pretreated with treated MG-132 (50 μM) for 30 min before exposure to IoP for 5 h. Proteasome inhibitor MG-132 blocked the degradation of IκBα in IoP-treated MOLT-4 cells (mean ± S.D., *n* = 3, Student's *t* test). No degradation of IκBα was shown in Jurkat cells. *C* = non-treated control. *E* and *F*, IoP induced significant reductions of WWOX phosphorylation at Tyr-33 and Tyr-287 in 2 h (mean ± S.D., *n* = 3). Phosphorylation at Ser-14 was significantly increased. Phosphorylation at Tyr-61 was barely detectable in MOLT-4. *G*, IoP induced translocation of p-ERK to the nuclei in MOLT-4, as shown in a representative time-course experiment using isolated cytosolic and nuclear fractions. No nuclear accumulation of NF-κB/p65 was shown.

umented (12, 26, 28). We determined whether WWOX colocalizes with IκBα and ERK (or ERK1/2). By confocal microscopy, endogenous IκBα colocalized with WWOX in the cytoplasm of resting MOLT-4 cells, and IoP decreased the colocalization (Fig. 4, *A* and *B*). Similarly, WWOX colocalized with ERK1 and ERK2 in MOLT-4 cells, and IoP decreased the colocalization with time of treatment (Fig. 4, *A* and *B*), suggesting their release from the mitochondria.

We then isolated the cytoplasmic and mitochondrial fractions from MOLT-4. WWOX, IκBα, and ERK were present in the cytoplasm and mitochondria (Fig. 4*C*). IoP rapidly decreased the protein levels of WWOX and its Tyr-33 phosphorylation in the mitochondria (Fig. 4*C*), suggesting release of these proteins from the mitochondria. In additional experiments, WWOX and IκBα were found in the isolated mitochon-

dria, and the protein levels were reduced during exposure to IoP for 1 h followed by increase after 2–3 h (Fig. 4*D*).

By confocal microscopy, IoP significantly reduced the mitochondrial localization of IκBα and WWOX in MOLT-4 (Fig. 4*E*), again suggesting their translocation to the cytoplasm from the mitochondria. In comparison, TNF-α did not effectively reduce the levels of WWOX in the mitochondria (Fig. 4*E*). However, TNF-α significantly decreased the level of mitochondrial IκBα (Fig. 4*E*).

WWOX Protected IκBα from Degradation—By co-immunoprecipitation, IκBα was shown to physically interact with WWOX and ERK in resting MOLT-4 (Fig. 5*A*). When cells were treated with half-strength IoP, ERK exhibited a delayed phosphorylation in 2 h, and this led to dissociation of the IκBα·ERK·WWOX complex (Fig. 5*A*). Malignant breast
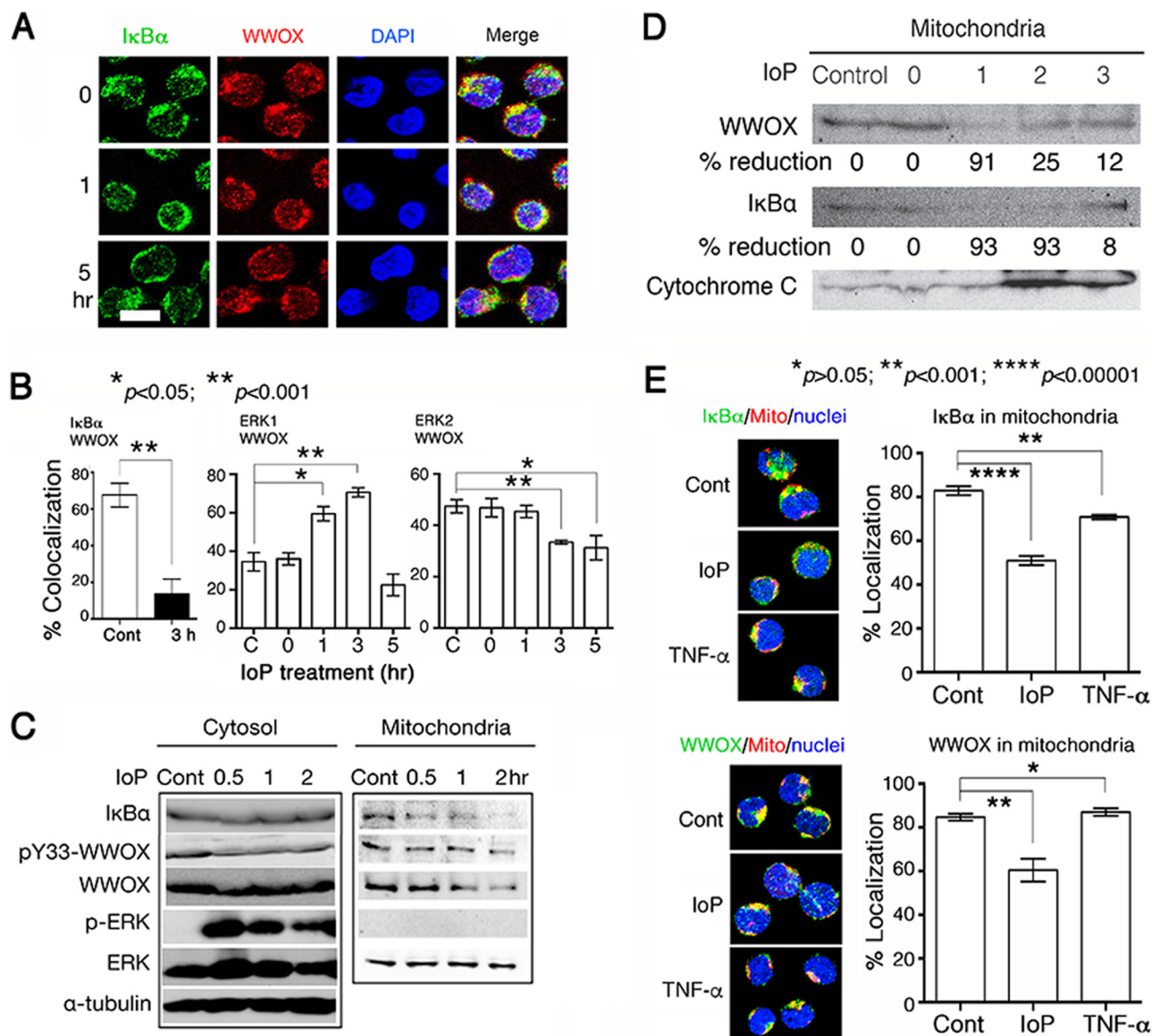
FIGURE 4. IoP decreased colocalization of WWOX and IκBα in the mitochondria. *A* and *B*, MOLT-4 cells were treated with IoP for the indicated times followed by processing fixation, permeabilization, and antibody staining for confocal microscopy. The nuclei were stained with DAPI. WWOX and IκBα colocalized in cytosol, and IoP significantly reduced the colocalization in 3 h (~200 cells counted, mean ± S.D., *n* = 3; Student's *t test*). Also, IoP decreased the colocalization of WWOX and ERK2 with time. In comparison, IoP increased the colocalization of WWOX and ERK1 initially followed by reduction. *C*, MOLT-4 cells were treated with IoP for the indicated times followed by preparing cytosolic and mitochondrial fractions. WWOX, ERK, and IκBα were present in the mitochondria. Mitochondrial IκBα was decreased upon IoP stimulation. *Cont* = non-treated control. *D*, similarly, IoP initially reduced the levels of WWOX and IκBα in the mitochondria followed by up-regulation with time. *E*, MOLT-4 cells were treated with IoP or TNF-α (50 ng/ml). Cells were processed for immunofluorescent staining and confocal microscopy. IoP induced the release of IκBα and WWOX from the mitochondria in 3 h; however, TNF-α was less effective (mean ± S.D., *n* = 3, Student's *t test*).

MDA-MB-231 cancer cells do not express WWOX (40), and IoP induced rapid IκBα degradation in 10 min (*top panel*; Fig. 5*B*). Ectopic expression of EGFP-WWOX in MDA-MB-231 resulted in blocking IoP-induced degradation of endogenous IκBα (*bottom panel*; Fig. 5*B*). PMA at 10 μM induced ERK phosphorylation in <1 min, and the phosphorylation led to rapid reduction of the IκBα·ERK·WWOX complex (Fig. 5*C*).

The Non-PEST Region of IκBα Physically Interacted with WWOX—The N-terminal ANK domain and the C-terminal PEST domain of IκBα physically bind NF-κB and p53, respectively (27, 41). We utilized yeast two-hybrid analysis (21–23) and FRET (26, 28, 42, 43) to map the domain/domain interac-

tions between WWOX and IκBα. By Cytotrap yeast two-hybrid assay, we determined that IκBα-(1–67) (amino acid #1–67) and the ankyrin domain of IκBα-(68–243) (amino acid #68–243) bound the full-length WWOX (Fig. 6, *A–D*). Yeast *cdc25* cells expressing Sos-tagged WWOX and Myr-tagged IκBα-(1–67) or IκBα-(68–243) were grown in the SD/galactose (−UL) plates at 22 and 37 °C. Positive binding allowed the growth of the *cdc25* mutant yeast at 37 °C due to activation of the Ras-signaling pathway (Fig. 6, *C* and *D*). Those results suggest that WWOX interacts with IκBα and may exert physiological functions in cells.

MOLT-4 cells were transiently overexpressed with EYFP-WWOX and ECFP-tagged IκBα, IκBα295N-(1–295), or
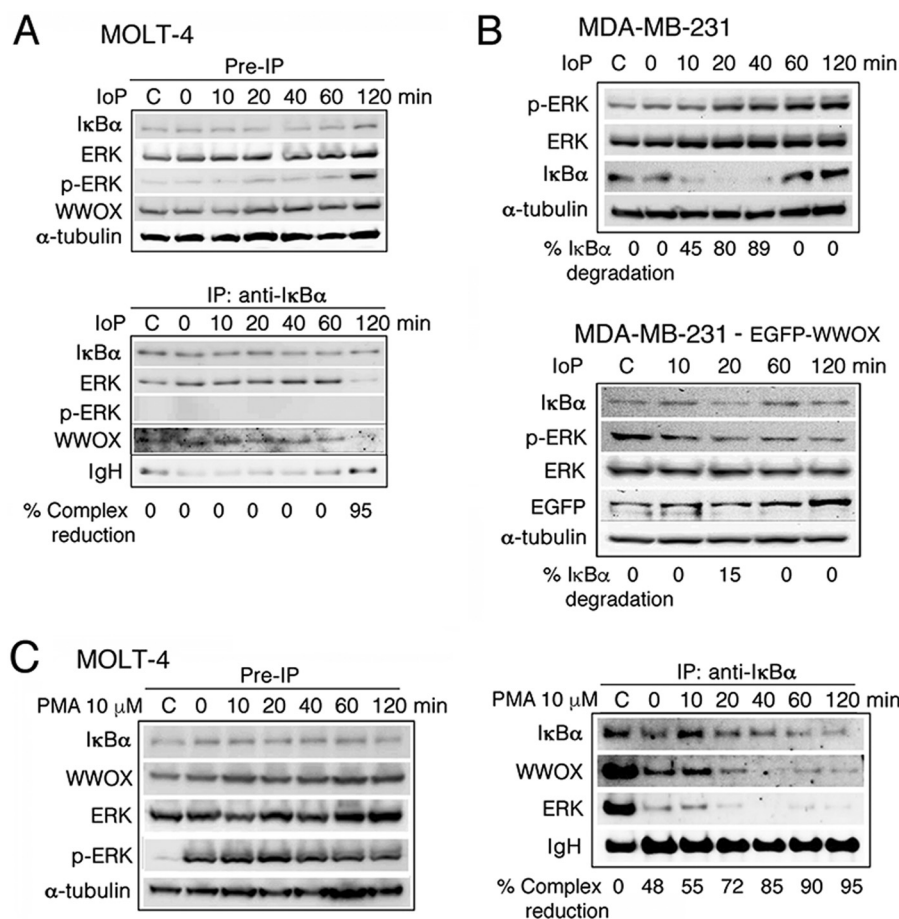
FIGURE 5. **WWOX protected IκBα from proteasomal degradation, and phosphorylated ERK increased WWOX/IκBα dissociation from the IκBα·ERK·WWOX complex.** *A*, by co-immunoprecipitation (*IP*), IκBα bound non-phosphorylated ERK and WWOX in resting MOLT-4 cells. The cells were stimulated with half-strength IoP. Upon ERK phosphorylation, the complex dissociation occurred. *C* = non-treated control. *IgH* = IgG heavy chain. *B*, IoP induced IκBα degradation in 10 min in WWOX-deficient MDA-MB-231 cells. Restoration with EGFP-WWOX in MDA-MB-231 cells prevented IoP-mediated IκBα degradation. *C*, the WWOX·ERK·IκBα complex was present in MOLT-4 cells. PMA alone rapidly activated ERK, which led to dissociation of the WWOX·ERK·IκBα complex.

IκBα243C-(244–295). By FRET microscopy, the N terminus of IκBα physically interacted with the full-length WWOX in MOLT-4, whereas the C-terminal PEST domain did not bind WWOX (Fig. 6*E*). In the negative control (EYFP *versus* ECFP), no binding interaction was observed (Fig. 6*E*). In addition, the N-terminal first WW domain of WWOX interacted with IκBα (Fig. 6*F*). In contrast, dominant-negative WWOX (dn-WWOX) did not bind IκBα (Fig. 6*F*). dn-WWOX possesses K28T/D29V alterations in the first WW domain (21). Also, dn-WWOX blocks the phosphorylation of WWOX at Tyr-33 and p53 at Ser-46 (21, 23). To further confirm the aforementioned results, we carried out co-immunoprecipitation and determined that endogenous IκBα bound ectopic EGFP-WWOX and endogenous non-phosphorylated ERK in MOLT-4, whereas IκBα did not bind ectopic dn-WWOX effectively (Fig. 6*G*). Notably, dn-WWOX increased IκBα/ERK binding by 1-fold. Together, the N-terminal first WW domain of WWOX physically interacts with ERK and the non-PEST area of IκBα.

To further verify the binding of WWOX to the non-PEST region of IκBα, HEK293 fibroblasts were transiently overexpressed with ECFP-tagged IκBα, IκBα295N, IκBα243C, or other indicated constructs (Fig. 7*A*). By co-immunoprecipitation, WWOX bound the full-length IκBα and the head/ANK-

containing IκBα-(1–243) but weakly with ANK-only IκBα-(68–243) (Fig. 7*B*). Moreover, WWOX bound the full-length IκBα and IκBα295N (head/ANK/PEST) but not the IκBα243C (PEST only) (Fig. 7*C*). The IκBα295N lacks a 19-amino acid tail at the C terminus. The IκBα243C possesses the C-terminal PEST domain. In addition, WWOX bound the N-terminal head IκBα-(1–67), which is in front of the ANK domain (Fig. 7*D*). Binding of WWOX with PEST occurred when linkers flanking the PEST-containing IκBα-(244–314) were added (Fig. 7*D*). Overall, WWOX binds to the non-PEST domain area of IκBα.

MEK1 Inhibitor U0126 Decreased the Binding of IκBα with WWOX—U0126 inhibited IoP-induced CD3 and CD8 expression in MOLT-4 cells (Fig. 2*C*). To investigate whether U0126 blocks the interactions between WWOX, IκBα, and ERK, co-immunoprecipitation was carried out. Again, IκBα physically bound WWOX and ERK in resting MOLT-4 cells, and IoP induced the dissociation of IκBα with WWOX and ERK in 2–3 h. U0126 disrupted the binding of IκBα with WWOX but not with ERK in MOLT-4 during pretreatment for 30 min (Fig. 7*E*). IoP and U0126 reduced the IκBα/ERK interaction with time (Fig. 7*E*).

The presence of the IκBα·ERK·WWOX complex in the spleen is shown (Fig. 7, *F–H*). By using whole spleen lysates
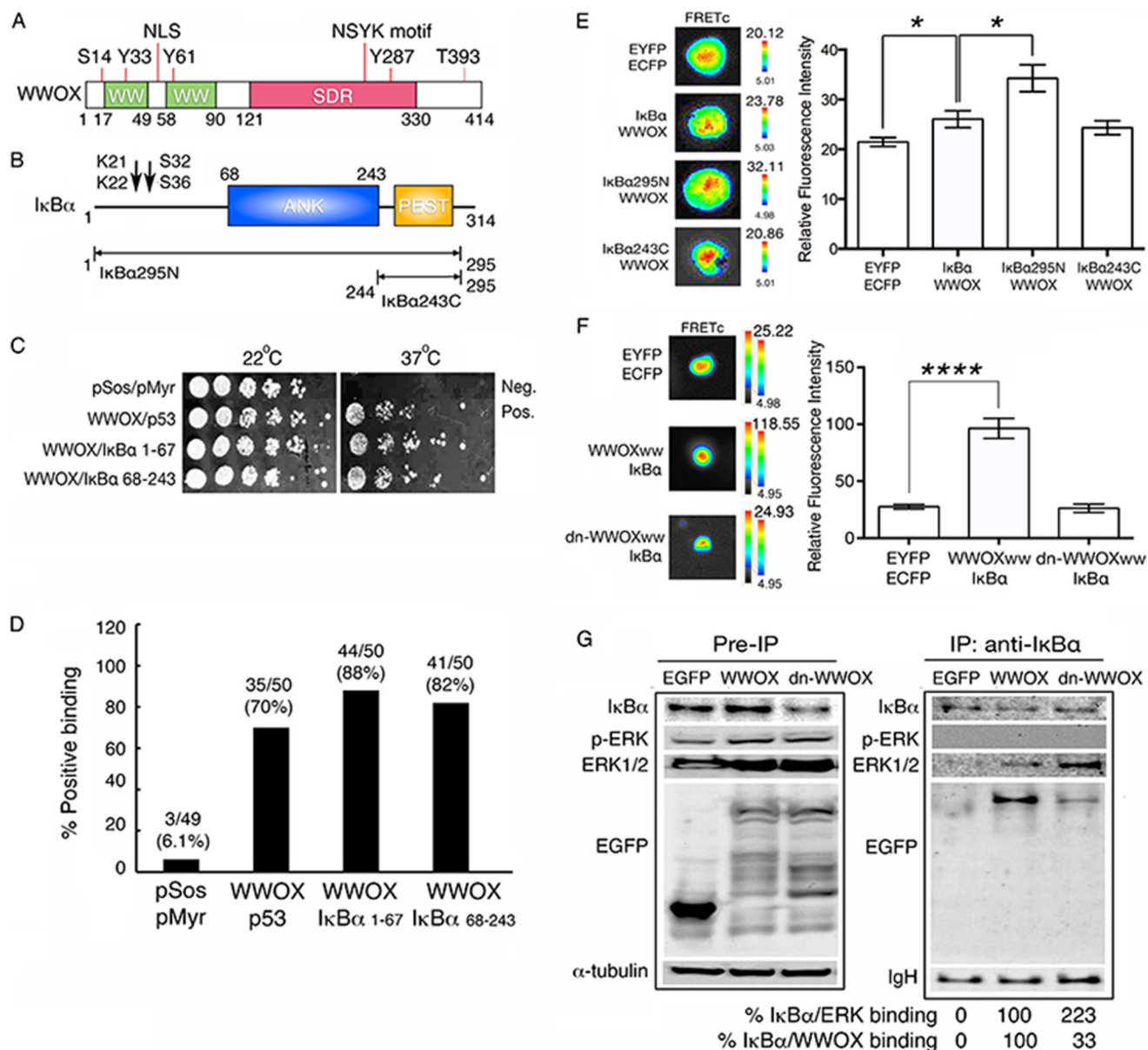
FIGURE 6. **The N-terminal WW domain of WWOX bound IκBα and ERK.** *A* and *B*, schematic graphs for the full-length WWOX and IκBα, respectively. Known phosphorylation sites are indicated in both proteins. Mono-ubiquitination sites Lys-21 and Lys-22 are shown for IκBα. *NLS* = nuclear localization signal. *C* and *D*, Cytotrap yeast two-hybrid analysis showed the positive binding of WWOX with IκBα 1–67 and IκBα 68–243, as reflected by yeast growth at 37 °C (in 1:2 serial dilutions). All yeast cells grow at room temperature. The binding activates the Ras pathway in *cdc25* mutant yeast that allows their growth at 37 °C. Binding of WWOX with p53 is regarded as positive controls. In negative controls, Sos protein did not bind the Myr tag expressed on the cell membrane. *E*, by FRET microscopy, EYFP-WWOX bound the N terminus of IκBα (ECFP-IκBα295N) but not the PEST domain (ECFP-IκBα243C) in MOLT-4 cells. Percent pixel changes for the strongest binding areas (*red color*) were quantified and tabulated (mean ± S.D., $n = 8$ for IκBα/WWOX, $n = 9$ for IκBα295N/WWOX, $n = 6$ for IκBα243C/WWOX; Student's *t* test; *, $p < 0.05$). In the negative control, ECFP did not bind EYFP. *F*, also, by FRET microscopy, EYFP-tagged the first WW domain (EYFP-WWOXww) physically bound ECFP-IκBα compared with the ECFP/EYFP controls (****, $p < 0.001$). A dominant-negative (*dn*) construct dn-WWOXww at the WW domain had a significantly reduced binding with IκBα (mean ± S.D., $n = 6$ for EYFP/ECFP, $n = 4$ for WWOXww/IκBα, $n = 5$ for dn-WWOXww/IκBα). *G*, HEK293 cells transiently overexpressed EGFP-WWOX or dominant-negative WWOX. By immunoprecipitation, IκBα was shown to bind ERK, p-ERK, and WWOX but not dn-WWOX. *Pre-IP* = $1/10$ of each of the whole cell lysates (~30 μg) was loaded onto gels. The extent of IκBα binding with ERK and WWOX was quantified.

from naïve BALB/c mice for co-immunoprecipitation, binding of IκBα with WWOX and ERK along with Tyr(P)-33-WWOX interacting with ERK, was found in the spleen lysates of naïve BALB/c mice.

Time-lapse FRET Microscopy of IκBα·ERK·WWOX Signaling—IoP stimulated rapid phosphorylation of IκBα and ERK in 5 min or less (Fig. 2*A*). By measuring three-way protein/protein interactions (29, 43), ECFP-IκBα was excited to allow the energy transfer from a high to a low level, *i.e.* to EGFP-ERK

and then to DsRed-monomer WWOX. Positive signals were observed in IoP-stimulated COS7 cells expressing ECFP-IκBα, EGFP-ERK, and DsRed-monomer WWOX (Fig. 8 and supplemental Video S1; 36 positive cells of 40 counted in end-point experiments). The emission energy from ECFP could not directly go to the recipient DsRed monomer without an EGFP bridge. The reason for using monomer expression for WWOX is that this protein may undergo self-binding during overexpression (data not shown).
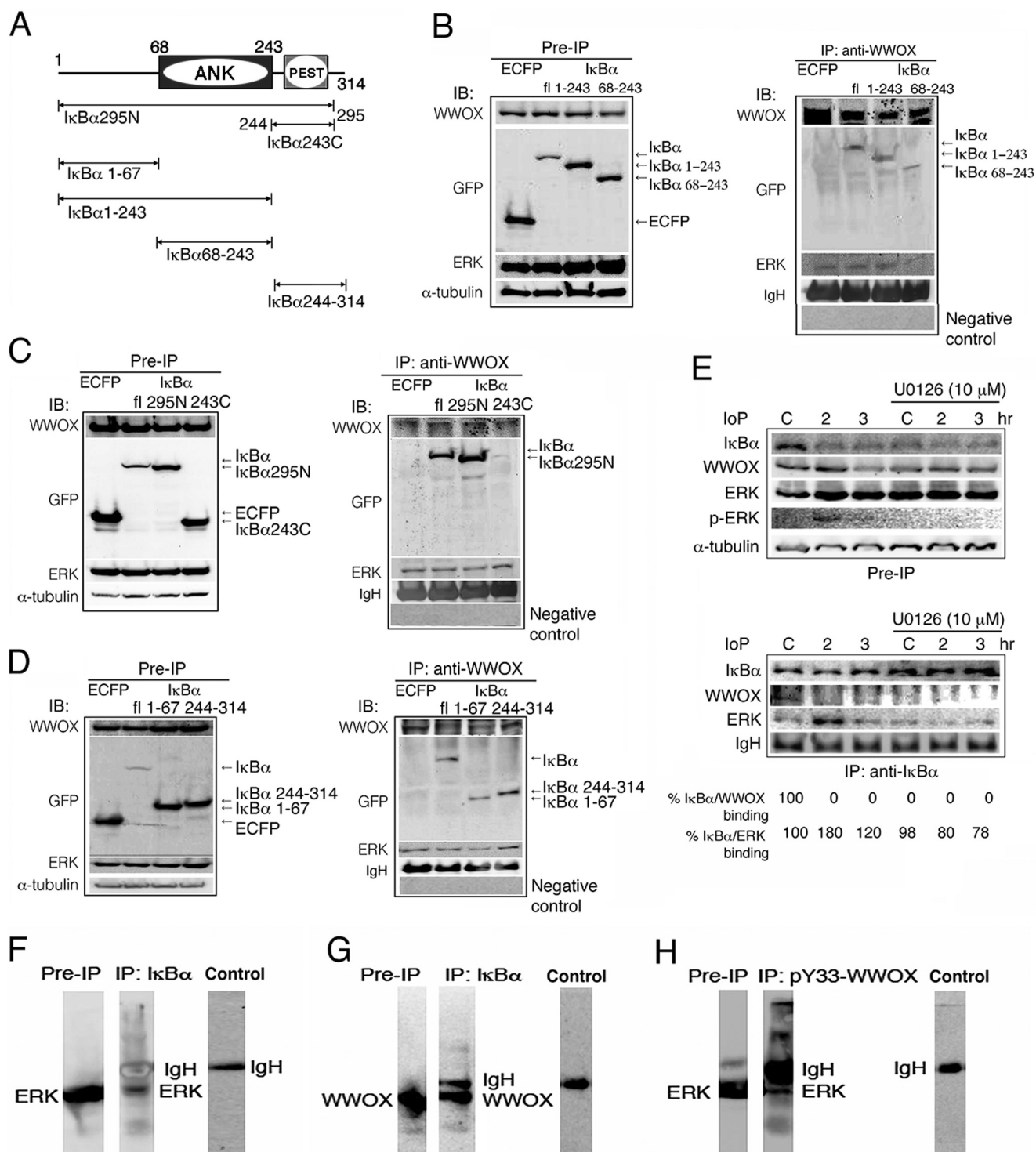
FIGURE 7. **WWOX bound the non-PEST region of IκBα.** *A*, HEK293 cells were transiently overexpressed with ECFP and ECFP-tagged constructs, respectively. After culturing for 48–72 h, WWOX was precipitated by a specific antibody as shown below. The GFP antibody, which cross-reacts with CFP, was used for probing the ECFP-tagged proteins. *B, C,* and *D,* by co-immunoprecipitation (*IP*), WWOX was shown to bind the full-length IκBα, IκBα295N, IκBα-(1–67), IκBα-(68–243), IκBα-(1–243), and IκBα-(244–314). WWOX did not bind the PEST-containing IκBα243C. Binding of WWOX with ERK was also shown. Negative control = non-immune IgG used for immunoprecipitation. *IB,* immunoblot. *E,* MOLT-4 cells were pretreated with U0126 (10 μM) for 30 min before exposure to IoP for indicated times. U0126 disrupted the binding of WWOX with ERK and IκBα. Similarly, IoP dissociated WWOX from the complex ERK and IκBα. U0126 and IoP in combination further reduced the binding of IκBα with ERK. *C* = non-treated control or resting cells. Pre-IP = 1/10 of each of the whole cell lysates (~30 μg) was loaded onto gels. Percent changes in binding were calculated as indicated. *F–H,* by using whole spleen lysates from naïve BALB/c mice for co-immunoprecipitation, IκBα interacted with WWOX and ERK, and Tyr(P)-33-WWOX interacted with ERK are shown. *Control* = non-immune serum used for immunoprecipitation.

When dominant-negative EGFP-ERK was used, no positive signals were observed (Fig. 8 and supplemental Video S2; negative signals in 38 cells of 40). Similarly, when dominant-negative WWOX was used, no signals were observed (Fig. 8 and supplemental Video S3; negative signals in 32 cells of 32). These observations suggested that functionally active
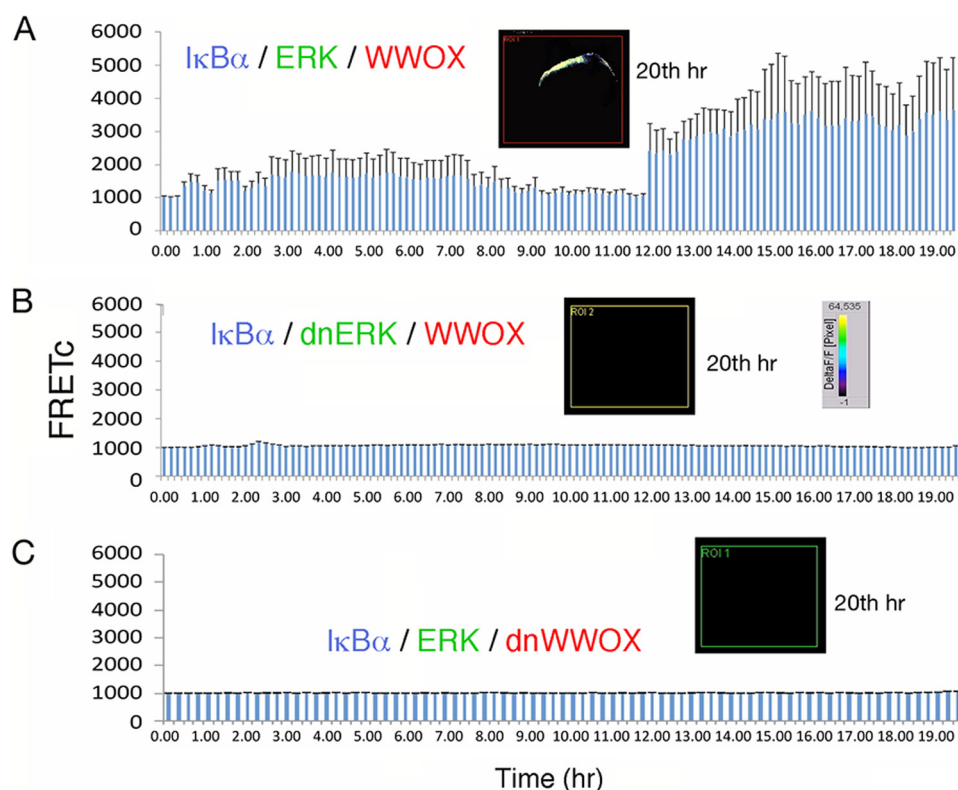
FIGURE 8. **Time-lapse FRET microscopy for IoP signaling.** *A*, COS7 cells were transiently overexpressed with ECFP-IκBα, EGFP-ERK, and DsRed-monomer WWOX and exposed to IoP for FRET imaging (also see supplemental Video S1). The *bar graph* is an average of two experiments and its range. *B*, the cells were also overexpressing ECFP-IκBα, EGFP-dnERK (dominant negative), and DsRed-monomer WWOX for FRET imaging (mean ± S.D., $n = 3$; also see supplemental Video S2). *FRETc*, FRET concentration. *C*, alternatively, the cells overexpressing ECFP-IκBα, EGFP-ERK, and DsRed-monomer dnWWOX were used for FRET imaging (mean ± S.D., $n = 3$; also see supplemental Video S3).

IκBα, ERK, and WWOX are needed to transduce the IoP signal.

In summary, an endogenous IκBα·ERK·Tyr(P)-33-WWOX complex is present in the immature MOLT-4 cells (Fig. 9). IoP induced rapid phosphorylation of endogenous ERK and IκBα in 5 min or less. Meanwhile, WWOX underwent dephosphorylation at Tyr-33 and Tyr-287 and phosphorylation at Ser-14 in 1–2 h, which led to dissociation of WWOX from the p-IκBα·p-ERK complex. Degradation of IκBα and de-phosphorylation of ERK occurred in the next 3–5 h and lasted for the next 12 h. Meanwhile, a portion of WWOX and ERK relocated to the nucleus. When the level of IκBα returned to normal, up-regulation of CD3 and CD8 along with re-formation of the IκBα·ERK·Tyr(P)-33-WWOX occurred in 15–24 h (Fig. 9).

Discussion

Here, we have discovered for the first time that an endogenous complex of Tyr(P)-33-WWOX, ERK, and IκBα plays a critical role in driving T cell acute lymphoblastic leukemia maturation. A portion of this complex is present in the mitochondria. We have previously reported the presence of WWOX and p53 in the mitochondria (22, 39, 44). In addition, WWOX is involved in mitochondrial respiration and metabolism (45, 46).

By co-immunoprecipitation, yeast two-hybrid analysis, time-lapse FRET microscopy, and expression of cloned plasmid vectors, we deciphered how the component proteins in the complex interact with each other and how the action contributes to MOLT-4 maturation. IoP rapidly stimulates phosphorylation

of ERK and IκBα in <5 min, and then endogenous WWOX undergoes significant dephosphorylation at Tyr-33 and Tyr-287 in 1–2 h in MOLT-4 along with significantly increased Ser-14 phosphorylation. WWOX then dissociates from ERK and IκBα in 1–2 h. Later, ERK becomes dephosphorylated to a basal level or non-phosphorylated, and p-IκBα is degraded in 3–15 h. Ultimately, CD3$^+$ and CD8$^+$ MOLT-4 cells are present in 15–24 h. There are 25% of cells are at the G_2/M phase of the cell cycle. ERK has been implicated in the growth factor-independent cell cycle progression toward the G_2/M phase (33). CD4$^+$ cells are barely detectable, although IoP may rapidly induce CD4 expression in 1–3 h followed by reduction (data not shown).

Supporting evidence is provided that there is a time-related release of WWOX and IκBα from the mitochondria in 1–2 h post IoP stimulation, whereas ERK appears to remain in the mitochondria. IκBα may undergo degradation upon release from mitochondria. We have recently reported the shuttling of TRAPPC6A (trafficking protein particle complex 6A) in between nucleolus and mitochondrion (42, 43). TRAPPC6A is a carrier for WWOX to undergo nuclear translocation. Whether IoP-induced translocation of WWOX and ERK to the nucleus requires TRAPPC6A remains to be established.

By using WWOX-negative MDA-MB-231 cells, we demonstrated that Tyr(P)-33-WWOX binds and prevents IκBα from degradation. WWOX binds to the non-PEST area of IκBα. Upon IκBα phosphorylation, WWOX becomes dissociated.
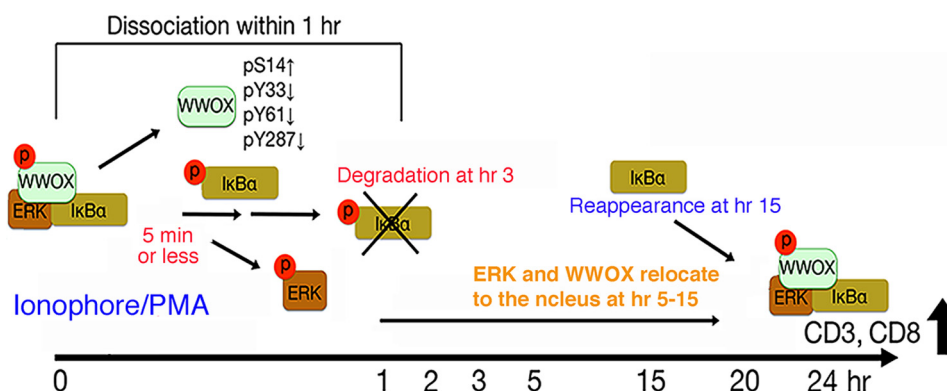
FIGURE 9. **IoP signaling.** A schematic graph is illustrated for IoP-induced signal transduction leading to MOLT-4 maturation. An endogenous IκBα·ERK·Tyr(P)-33-WWOX complex is present in the immature MOLT-4. IoP rapidly induces ERK and IκBα phosphorylation in 5 min or less, and then WWOX undergoes dephosphorylation at Tyr-33 and Tyr-287 and phosphorylation at Ser-14. WWOX is released from the p-ERK·p-IκBα complex in 1 h. p-IκBα is then degraded, and ERK phosphorylation returns to a basal level or non-phosphorylation in 5–15 h. Meanwhile, both ERK and WWOX relocate to the nucleus (to induce gene transcription for cell maturation). Finally, expression of CD3 and CD8 occurs along with reappearance of the IκBα·ERK·WWOX complex in the cells in 15–24 h. CD4 is barely detectable.

Similarly, p-ERK interacts with p-IκBα, which lasts for 2 h. The interaction blocks the degradation of p-IκBα. Clearly, the initial events for IκBα, ERK, and WWOX are needed for MOLT-4 maturation.

Together, both WWOX and ERK protect IκBα from degradation. Phosphorylation of IκBα and ERK along with altered WWOX phosphorylation destabilizes the IκBα·ERK·WWOX complex. p-ERK apparently has a conformal change that allows its dissociation from the IκBα·ERK·WWOX complex.

WWOX and ERK relocate to the nucleus 5 h post IoP exposure, suggesting that both proteins are committed to MOLT-4 maturation by working in the nucleus. It has been well documented that activated ERK controls the activity of many transcription factors. The N-terminal first WW domain of WWOX induces transcriptional activation of NF-κB, and WWOX interacts with many transcription factors to control neuronal survival via its WW domain *in vivo* (28).

We have shown that a portion of cytosolic WWOX binds membrane Hyal-2, as determined by co-immunoprecipitation, confocal microscopy, FRET microscopy, and electron microscopy (26). Immuoelectron micrographs showed the membrane exposure of WWOX to the extracellular matrix (26). WWOX does not have a membrane-localization domain. WWOX is anchored on the membrane by binding with Hyal-2 (26), Ezrin (47, 48), and other membrane proteins. WWOX is involved in the TGF-β signaling (26, 42, 43, 49). Whether IoP cross-talks with TGF-β signaling and activates membrane Hyal-2/WWOX remains to be established.

How Ser(P)-14-WWOX works *in vivo* is largely unknown. In our preliminary study, we made Ser-14-phosphorylated and non-phosphorylated WWOX peptides of 15 amino acid residues and found that the phosphorylated peptide is a potent inducer of T cell expansion in BALB/c mice growing with melanoma.[3] The T cells include CD3+, CD4+, and CD8+ populations. Without phosphorylation, there is no induction of T cells, again suggesting a role of pSer-14-WWOX in committing T cell grow and expansion *in vivo*.

The WW, ANK and PEST domains are involved in signal transduction (13, 26, 27, 33, 37, 48–52). We have extensively investigated how WWOX binds IκBα and determined that the first N-terminal WW domain binds the non-PEST region in IκBα. First, binding of WWOX with IκBα is shown in yeast two-hybrid analysis. Second, by FRET analysis, the N terminus of IκBα interacts much stronger with WWOX than the C-terminal PEST domain. A dominant-negative WWOX construct possessing alterations in the WW domain loses its binding with IκBα, indicating that the N-terminal first WW domain of WWOX interacts with the N-terminal ankyrin-repeat motif of IκBα. By co-immunoprecipitation, the binding interactions are confirmed by using designed expression constructs of IκBα for interacting with WWOX. Finally, time-lapse FRET analysis confirms that functionally active IκBα, ERK, and WWOX together are critical for IoP signaling and MOLT-4 maturation.

Tyrosine phosphorylation is known in many WW domain-containing proteins (52). Unknown kinases and phosphatases are involved in the IoP-mediated phosphorylation and dephosphorylation in WWOX. We have utilized specific inhibitors to block the function of ERK and IκBα, and the inhibition leads to blockade of MOLT-4 maturation. As a partner of WWOX (21–23), p53 participates in T cell maturation (53). However, the precise molecular action needs further investigation.

Inhibition of MEK kinase by U0126 results in blocking of ERK phosphorylation and MOLT-4 maturation. Whether MEK is in the IκBα·ERK·WWOX complex is unknown. Indeed, WWOX physically binds MEK in many types of cancer cells (12). Dissociation of the WWOX·MEK complex by high concentrations of PMA allows WWOX relocation to the mitochondria for causing cancer cell death. IκBα is a key inhibitor of NF-κB (7, 54) and appears to play an inhibitor role in preventing the phosphorylation of ERK in response to IoP. Thus, blocking of IκBα degradation by proteasome inhibitor MG132 halts MOLT-4 maturation.

In addition to MOLT-4, we investigated whether IoP induces maturation in monocytic U937 and THP-1 cells. The less differentiated U937 is susceptible to IoP for induction of CD8α. Unlike MOLT-4 and Jurkat T cells, monocytic cells undergo an early and a late phase of ERK phosphorylation. Functional rel-

---

[3] Y.-A. Chen, C.-Y. Lu, W.-J. Wang, J.-Y. Chang, and N.-S. Chang, manuscript in preparation.

evance for ERK phosphorylation remains to be established. Taken together, immature leukemia cells are susceptible to maturation by IoP. This raises promising therapeutic considerations and designing approaches to induce leukemia cell maturation in patients.

References

1. Starr, T. K., Jameson, S. C., and Hogquist, K. A. (2003) Positive and negative selection of T cells. *Annu. Rev. Immunol.* **21,** 139 –176

2. Koch, U., and Radtke, F. (2011) Mechanisms of T cell development and transformation. *Annu. Rev. Cell Dev. Biol.* **27,** 539 –562

3. Bottero, V., Withoff, S., and Verma, I. M. (2006) NF-κB and the regulation of hematopoiesis. *Cell Death Differ.* **13,** 785 –797

4. Zhu, M.X., Wan, W.L., Li, H.S., Wang, J., Chen, G.A., and Ke, X.Y. (2015) Thymopentin enhances the generation of T-cell lineage derived from human embryonic stem cells *in vitro. Exp. Cell Res.* **331,** 387 –398

5. Anderson, G., Baik, S., Cowan, J.E., Holland, A.M., McCarthy, N.I., Nakamura, K., Parnell, S.M., White, A.J., Lane, P.J., Jenkinson, E.J., and Jenkinson, W.E. (2014) Mechanisms of thymus medulla development and function. *Curr. Top. Microbiol. Immunol.* **373,** 19 – 47

6. Zúñiga-Pflücker, J. C., and Lenardo, M. J. (1996) Regulation of thymocyte development from immature progenitors. *Curr. Opin. Immunol.* **8,** 215 –224

7. Jacobs, M. D., and Harrison, S. C. (1998) Structure of an IκBα/NF-κB complex. *Cell* **95,** 749 –758

8. Bakker, T. R., Renno, T., and Jongeneel, C. V. (1999) Impaired fetal thymocyte development after efficient adenovirus-mediated inhibition of NF-κB activation. *J. Immunol.* **162,** 3456 –3462

9. Hettmann, T., and Leiden, J. M. (2000) NF-κB is required for the positive selection of CD8+ thymocytes. *J. Immunol.* **165,** 5004 –5010

10. Iwata, M., Kuwata, T., Mukai, M., Tozawa, Y., and Yokoyama, M. (1996) Differential induction of helper and killer T cells from isolated CD4+CD8+ thymocytes in suspension culture. *Eur. J. Immunol.* **26,** 2081 –2086

11. Takahama, Y., and Nakauchi, H. (1996) Phorbol ester and calcium ionophore can replace TCR signals that induce positive selection of CD4 T cells. *J. Immunol.* **157,** 1508 –1513

12. Lin, H. P., Chang, J. Y., Lin, S. R., Lee, M. H., Huang, S. S., Hsu, L. J., and Chang, N. S. (2011) Identification of an *in vivo* MEK/WOX1 complex as a master switch for apoptosis in T cell leukemia. *Genes Cancer* **2,** 550 –562

13. Chang, N. S., Hsu, L. J., Lin, Y. S., Lai, F. J., and Sheu, H. M. (2007) WW domain-containing oxidoreductase: a candidate tumor suppressor. *Trends Mol. Med.* **13,** 12 –22

14. Chang, J. Y., He, R. Y., Lin, H. P., Hsu, L. J., Lai, F. J., Hong, Q., Chen, S. J., and Chang, N. S. (2010) Signaling from membrane receptors to tumor suppressor WW domain-containing oxidoreductase. *Exp. Biol. Med. (Maywood)* **235,** 796 – 804

15. Chang, H. T., Liu, C. C., Chen, S. T., Yap, Y. V., Chang, N. S., and Sze, C. I. (2014) WW domain-containing oxidoreductase in neuronal injury and neurological diseases. *Oncotarget* **5,** 11792 –11799

16. Chang, N. S. (2015) Introduction to a thematic issue for WWOX. *Exp. Biol. Med. (Maywood)* **240,** 281 –284

17. Abu-Remaileh, M., and Aqeilan, R. I. (2015) The tumor suppressor WW domain-containing oxidoreductase modulates cell metabolism. *Exp. Biol. Med. (Maywood)* **240,** 345 –350

18. Schrock, M. S., and Huebner, K. (2015) WWOX: a fragile tumor suppressor. *Exp. Biol. Med. (Maywood)* **240,** 296 –304

19. Sze, C. I., Kuo, Y. M., Hsu, L. J., Fu, T. F., Chiang, M. F., Chang, J. Y., and Chang, N. S. (2015) A cascade of protein aggregation bombards mitochondria for neurodegeneration and apoptosis under WWOX deficiency. *Cell Death Dis.* **6,** e1881

20. Chang, Y., Lan, Y. Y., Hsiao, J. R., and Chang, N. S. (2015) Strategies of oncogenic microbes to deal with WW domain-containing oxidoreductase. *Exp. Biol. Med. (Maywood)* **240,** 329 –337

21. Chang, N. S., Doherty, J., and Ensign, A. (2003) JNK1 physically interacts with WW domain-containing oxidoreductase (WOX1) and inhibits WOX1-mediated apoptosis. *J. Biol. Chem.* **278,** 9195 –9202

22. Chang, N. S., Pratt, N., Heath, J., Schultz, L., Sleve, D., Carey, G. B., and Zevotek, N. (2001) Hyaluronidase induction of a WW domain-containing oxidoreductase that enhances tumor necrosis factor cytotoxicity. *J. Biol. Chem.* **276,** 3361 –3370

23. Chang, N. S., Doherty, J., Ensign, A., Schultz, L., Hsu, L. J., and Hong, Q. (2005) WOX1 is essential for tumor necrosis factor-, UV light-, staurosporine-, and p53-mediated cell death, and its tyrosine 33-phosphorylated form binds and stabilizes serine 46-phosphorylated p53. *J. Biol. Chem.* **280,** 43100 – 43108

24. Chen, S. J., Lin, P. W., Lin, H. P., Huang, S. S., Lai, F. J., Sheu, H. M., Hsu, L. J., and Chang, N. S. (2015) UV irradiation/cold shock-mediated apoptosis is switched to bubbling cell death at low temperatures. *Oncotarget* **6,** 8007 – 8018

25. Hong, Q., Sze, C. I., Lin, S. R., Lee, M. H., He, R. Y., Schultz, L., Chang, J. Y., Chen, S. J., Boackle, R. J., Hsu, L. J., and Chang, N. S. (2009) Complement C1q activates tumor suppressor WWOX to induce apoptosis in prostate cancer cells. *PLoS ONE* **4,** e5755

26. Hsu, L. J., Schultz, L., Hong, Q., Van Moer, K., Heath, J., Li, M. Y., Lai, F. J., Lin, S. R., Lee, M. H., Lo, C. P., Lin, Y. S., Chen, S. T., and Chang, N. S. (2009) Transforming growth factor β1 signaling via interaction with cell surface Hyal-2 and recruitment of WWOX/WOX1. *J. Biol. Chem.* **284,** 16049 –16059

27. Chang, N. S. (2002) The non-ankyrin C terminus of IκBα physically interacts with p53 *in vivo* and dissociates in response to apoptotic stress, hypoxia, DNA damage, and transforming growth factor-β1-mediated growth suppression. *J. Biol. Chem.* **277,** 10323 –10331

28. Li, M. Y., Lai, F. J., Hsu, L. J., Lo, C. P., Cheng, C. L., Lin, S. R., Lee, M. H., Chang, J. Y., Subhan, D., Tsai, M. S., Sze, C. I., Pugazhenthi, S., Chang, N. S., and Chen, S. T. (2009) Dramatic co-activation of WWOX/WOX1 with CREB and NF-κB in delayed loss of small dorsal root ganglion neurons upon sciatic nerve transection in rats. *PLoS ONE* **4,** e7820

29. Lee, M. H., Lin, S. R., Chang, J. Y., Schultz, L., Heath, J., Hsu, L. J., Kuo, Y. M., Hong, Q., Chiang, M. F., Gong, C. X., Sze, C. I., and Chang, N. S. (2010) TGF-β induces TIAF1 self-aggregation via type II receptor-independent signaling that leads to generation of amyloid β plaques in Alzheimer's disease. *Cell Death Dis.* **1,** e110

30. van Dongen, J. J., Krissansen, G. W., Wolvers-Tettero, I. L., Comans-Bitter, W. M., Adriaansen, H. J., Hooijkaas, H., van Wering, E. R., and Terhorst, C. (1988) Cytoplasmic expression of the CD3 antigen as a diagnostic marker for immature T-cell malignancies. *Blood* **71,** 603 – 612

31. Tanahashi, M., Yokoyama, T., Kobayashi, Y., Yamakawa, Y., Maeda, M., and Fujii, Y. (2001) Effect of phorbol ester and calcium ionophore on human thymocytes. *Hum. Immunol.* **62,** 771 –781

32. He, H., Wang, X., Gorospe, M., Holbrook, N. J., and Trush, M. A. (1999) Phorbol ester-induced mononuclear cell differentiation is blocked by the mitogen-activated protein kinase kinase (MEK) inhibitor PD98059. *Cell Growth Differ.* **10,** 307 –315

33. Torii, S., Yamamoto, T., Tsuchiya, Y., and Nishida, E. (2006) ERK MAP kinase in G cell cycle progression and cancer. *Cancer Sci.* **97,** 697 –702

34. Yamamoto, T., Ebisuya, M., Ashida, F., Okamoto, K., Yonehara, S., and Nishida, E. (2006) Continuous ERK activation downregulates antiproliferative genes throughout G_1 phase to allow cell-cycle progression. *Curr. Biol.* **16,** 1171 –1182

35. Gibbings, D.J., Marcet-Palacios, M., Sekar, Y., Ng, M.C., and Befus, A.D.

(2007) CD8α is expressed by human monocytes and enhances Fcγ R-dependent responses. *BMC Immunol.* **8,** 12

36. Mahajan, N. P., Whang, Y. E., Mohler, J. L., and Earp, H. S. (2005) Activated tyrosine kinase Ack1 promotes prostate tumorigenesis: role of Ack1 in polyubiquitination of tumor suppressor Wwox. *Cancer Res.* **65,** 10514–10523

37. Ludes-Meyers, J. H., Kil, H., Bednarek, A. K., Drake, J., Bedford, M. T., and Aldaz, C. M. (2004) WWOX binds the specific proline-rich ligand PPXY: identification of candidate interacting proteins. *Oncogene* **23,** 5049–5055

38. Lai, F. J., Cheng, C. L., Chen, S. T., Wu, C. H., Hsu, L. J., Lee, J. Y., Chao, S. C., Sheen, M. C., Shen, C. L., Chang, N. S., and Sheu, H. M. (2005) WOX1 is essential for UVB irradiation-induced apoptosis and down-regulated via translational blockade in UVB-induced cutaneous squamous cell carcinoma *in vivo. Clin. Cancer Res.* **11,** 5769–5777

39. Hsu, L.J., Hong, Q., Schultz, L., Kuo, E., Lin, S.R., Lee, M.H., Lin, Y.S., and Chang, N.S. (2008) Zfra is an inhibitor of Bcl-2 expression and cytochrome c release from the mitochondria. *Cell Signal.* **20,** 1303–1312

40. Chang, N.S., Schultz, L., Hsu, L.J., Lewis, J., Su, M., and Sze CI. (2005) 17β-Estradiol upregulates and activates WOX1/WWOXv1 and WOX2/WWOXv2 *in vitro*: potential role in cancerous progression of breast and prostate to a premetastatic state *in vivo. Oncogene* **24,** 714–723

41. Perkins, N. D. (2007) Integrating cell-signalling pathways with NF-κB and IKK function. *Nat. Rev. Mol. Cell Biol.* **8,** 49–62

42. Chang, J. Y., and Chang, N. S. (2015) WWOX dysfunction induces sequential aggregation of TRAPPC6AΔ, TIAF1, tau, amyloid β and apoptosis. *Cell Death Discov.* **1,** 15003

43. Chang, J. Y., Chiang, M. F., Lin, S. R., Lee, M. H., He, H., Chou, P. Y., Chen, S. J., Chen, Y. A., Yang, L. Y., Lai, F. J., Hsieh, C. C., Hsieh, T. H., Sheu, H. M., Sze, C. I., and Chang, N. S. (2012) TIAF1 self-aggregation in peritumor capsule formation, spontaneous activation of SMAD-responsive promoter in p53-deficient environment, and cell death. *Cell Death Dis.* **3,** e302

44. Chang, N.S. (2002) A potential role of p53 and WOX1 in mitochondrial apoptosis (review). *Int. J. Mol. Med.* **9,** 19–24

45. Abu-Remaileh, M., Joy-Dodson, E., Schueler-Furman, O., and Aqeilan RI. (2015) Pleiotropic functions of tumor suppressor WWOX in normal and cancer cells. *J. Biol. Chem.* **290,** 30728–30735

46. Choo, A., O'Keefe, L.V., Lee, C.S., Gregory, S.L., Shaukat, Z., Colella, A., Lee, K., Denton, D., and Richards, R.I. (2015) Tumor suppressor WWOX moderates the mitochondrial respiratory complex. *Genes Chromosomes Cancer* **54,** 745–761

47. Jin, C., Ge, L., Ding, X., Chen, Y., Zhu, H., Ward, T., Wu, F., Cao, X., Wang, Q., and Yao, X. (2006) PKA-mediated protein phosphorylation regulates ezrin-WWOX interaction. *Biochem. Biophys. Res. Commun.* **341,** 784–791

48. Iessi, E., Zischler, L., Etringer, A., Bergeret, M., Morlé, A., Jacquemin, G., Morizot, A., Shirley, S., Lalaoui, N., Elifio-Esposito, S. L., Fais, S., Garrido, C., Solary, E., and Micheau, O. (2015) Death receptor-induced apoptosis signalling regulation by ezrin is cell type dependent and occurs in a DISC-independent manner in colon cancer cells. *PLoS ONE* **10,** e0126526

49. Ferguson, B. W., Gao, X., Zelazowski, M. J., Lee, J., Jeter, C. R., Abba, M. C., and Aldaz, C. M. (2013) The cancer gene WWOX behaves as an inhibitor of SMAD3 transcriptional activity via direct binding. *BMC Cancer* **13,** 593

50. Sze, C. I., Su, M., Pugazhenthi, S., Jambal, P., Hsu, L. J., Heath, J., Schultz, L., and Chang, N. S. (2004) Down-regulation of WW domain-containing oxidoreductase induces Tau phosphorylation *in vitro*: a potential role in Alzheimer's disease. *J. Biol. Chem.* **279,** 30498–30506

51. Dodson, E. J., Fishbain-Yoskovitz, V., Rotem-Bamberger, S., and Schueler-Furman, O. (2015) Versatile communication strategies among tandem WW domain repeats. *Exp. Biol. Med. (Maywood)* **240,** 351–360

52. Reuven, N., Shanzer, M., and Shaul, Y. (2015) Tyrosine phosphorylation of WW proteins. *Exp. Biol. Med. (Maywood)* **240,** 375–382

53. Martin-Blanco, N. M., Checquolo, S., Del Gaudio, F., Palermo, R., Franciosa, G., Di Marcotullio, L., Gulino, A., Canelles, M., and Screpanti, I. (2014) Numb-dependent integration of pre-TCR and p53 function in T-cell precursor development. *Cell Death Dis.* **5,** e1472

54. Chen, S. J., Huang, S. S., and Chang, N. S. (2013) Role of WWOX and NF-κB in lung cancer progression. *Transl. Respir. Med.* **1,** 15